Atmospheric methane variability: Centennial-scale signals in the Last Glacial Period

Rachael H. Rhodes, Edward J. Brook, Joseph R. Mcconnell, Thomas Blunier, Louise C. Sime, Xavier Faïn, Robert Mulvaney

AGU PUBLICATIONS

Global Biogeochemical Cycles

RESEARCH ARTICLE
10.1002/2016GB005570

Key Points:
- Novel centennial-scale atmospheric methane variability observed in Last Glacial to early Holocene of WAIS Divide ice core
- Methane variability characterized by recurrence intervals within broad 80–500 year range and mean peak-to-peak amplitudes of 16 ppb
- Amplitude of centennial-scale signal in stadial and interstadial periods is proportional to underlying millennial-scale CH_4 concentration

Supporting Information:
- Supporting Information S1

Correspondence to:
R. H. Rhodes,
rhr34@cam.ac.uk

Citation:
Rhodes, R. H., E. J. Brook, J. R. McConnell, T. Blunier, L. C. Sime, X. Faïn, and R. Mulvaney (2017), Atmospheric methane variability: Centennial-scale signals in the Last Glacial Period, *Global Biogeochem. Cycles*, *31*, 575–590, doi:10.1002/2016GB005570.

Received 4 NOV 2016
Accepted 6 MAR 2017
Accepted article online 14 MAR 2017
Published online 22 MAR 2017

Atmospheric methane variability: Centennial-scale signals in the Last Glacial Period

Rachael H. Rhodes[1], Edward J. Brook[2], Joseph R. McConnell[3], Thomas Blunier[4], Louise C. Sime[5], Xavier Faïn[6], and Robert Mulvaney[5]

[1]Department of Earth Sciences, University of Cambridge, Cambridge, UK, [2]College of Earth, Ocean and Atmospheric Sciences, Oregon State University, Corvallis, Oregon, USA, [3]Division of Hydrologic Sciences, Desert Research Institute, Reno, Nevada, USA, [4]Center for Ice and Climate, Niels Bohr Institute, University of Copenhagen, Copenhagen, Denmark, [5]British Antarctic Survey, Natural Environment Research Council, Cambridge, UK, [6]Université Grenoble Alpes, CNRS, IRD, Grenoble INP, IGE, Grenoble, France

Abstract In order to understand atmospheric methane (CH_4) biogeochemistry now and in the future, we must apprehend its natural variability, without anthropogenic influence. Samples of ancient air trapped within ice cores provide the means to do this. Here we analyze the ultrahigh-resolution CH_4 record of the West Antarctic Ice Sheet Divide ice core 67.2–9.8 ka and find novel, atmospheric CH_4 variability at centennial time scales throughout the record. This signal is characterized by recurrence intervals within a broad 80–500 year range, but we find that age-scale uncertainties complicate the possible isolation of any periodic frequency. Lower signal amplitudes in the Last Glacial relative to the Holocene may be related to incongruent effects of firn-based signal smoothing processes. Within interstadial and stadial periods, the peak-to-peak signal amplitudes vary in proportion to the underlying millennial-scale oscillations in CH_4 concentration—the relative amplitude change is constant. We propose that the centennial CH_4 signal is related to tropical climate variability that influences predominantly low-latitude wetland CH_4 emissions.

Plain Language Summary Using a new method to measure methane concentrations of ancient air trapped in ice cores, we have detected variability in atmospheric methane concentration on centennial time scales in the Last Glacial Period for the first time. We know these signals represent past changes in atmospheric methane because they appear in several ice core records. We propose that changes in methane emissions from tropical wetlands are responsible. How this new variability might be related to similar signals found in the late Holocene ice core records and the instrumental record of atmospheric methane is an open question.

1. Introduction

Accurately predicting the future evolution of atmospheric methane (CH_4) is critical because methane is a significant greenhouse gas that currently accounts for 17% of the radiative forcing from all long-lived greenhouse gases [*Myhre et al.*, 2013]. While the unprecedented ~2.5-fold increase in atmospheric methane since the industrialization of the western world can be linked to anthropogenic activity, other unexplained trends, superimposed on this rise, have been observed over the last few decades [*Dlugokencky et al.*, 2009; *Nisbet et al.*, 2016]. For example, the high atmospheric methane growth rates of the 1980s, equivalent to 1% growth each year, were followed by a decade of near-zero growth before methane levels increased again from 2006. These decadal-scale changes in methane growth rate have been attributed to many factors including variability in natural wetland emissions [*Kirschke et al.*, 2013; *Saunois et al.*, 2016], bacterial activity associated with agriculture [*Schaefer et al.*, 2016; *Schwietzke et al.*, 2016], and anthropogenic fossil fuel emission rates [*Aydin et al.*, 2011; *Rice et al.*, 2016; *Schaefer et al.*, 2016; *Schwietzke et al.*, 2016]. Recently, climate-sensitive biogenic emissions from agriculture or wetlands have been identified as the most probable causes of the post-2006 methane rise by *Schaefer et al.* [2016] with *Nisbet et al.* [2016] emphasizing the contribution of such emissions from the tropics in particular. In summary, even with extensive atmospheric monitoring programs, it is difficult to attribute fluctuations in atmospheric methane to variability in a specific source or sink. This problem is compounded in the observational era by significant anthropogenic emissions that may mask natural variability.

Preindustrial Holocene (pre-1850 A.D.) atmospheric methane records from polar ice cores also exhibit multidecadal variability [*Ferretti et al.*, 2005; *MacFarling Meure et al.*, 2006; *Mitchell et al.*, 2011; *Rhodes et al.*, 2013,

2016]. Here too, it has proved challenging to distinguish between variability in CH_4 emissions resulting from natural, climate-related forcing (e.g., influence of precipitation and temperature on wetland emissions) and anthropogenic forcing (e.g., influence of agricultural practices). Two tools can be used to help identify the origin of CH_4 variability: the interpolar difference and isotopic ratios δD and $\delta^{13}C$. Both suggest that climate-related emissions from Southern Hemisphere wetlands and anthropogenic emissions from the Northern Hemisphere jointly influenced the broad upward trend in CH_4 over the preindustrial Holocene [*Ferretti et al*., 2005; *Mitchell et al*., 2013]. While the interpolar difference across individual multidecadal features has not been investigated, *Sapart et al*. [2012] suggested that multidecadal variations in $\delta^{13}C$ could be linked to changes in pyrogenic and biogenic CH_4 sources, potentially connected to climatic phenomena such as the Medieval Climate Anomaly or to human phenomena such as the fall of the Roman empire. Potential past changes in the strength of the main CH_4 sink, destruction by OH radicals in the atmosphere, must also be considered. This is well constrained by atmospheric measurements for the past few decades [*Montzka et al*., 2011], but beyond this, we have to rely on atmospheric chemistry models that suggest little change in sink strength has occurred since the Last Glacial [*Levine et al*., 2011; *Murray et al*., 2014].

In order to isolate the natural CH_4 variability from human-influenced changes, CH_4 data are required from a time period free from anthropogenic influence and polar ice cores provide these records. Additionally, ice core CH_4 records allow us to investigate how CH_4 variability at the centennial-scale interacts with major climatic transitions, such as glacial-interglacial cycles. Ice core CH_4 data of sufficiently high temporal resolution and level of precision have become available recently due to analytical advances utilizing laser spectroscopy [*Stowasser et al*., 2012].

Here we investigate novel, centennial-scale, CH_4 variability during the recent deglaciation and Last Glacial Period (67.2–9.8 ka before present (B.P.) (1950 A.D.)) resolved within the ultrahigh-resolution continuous CH_4 record from the WAIS (West Antarctic Ice Sheet) Divide (WD) ice core [*Rhodes et al*., 2015]. Thus far, only the millennial-scale features of this record have been examined, revealing new abrupt features attributed to Hudson Strait Heinrich events [*Rhodes et al*., 2015] and constraining timings of the bipolar seesaw mechanism of abrupt climate change [*West Antarctic Ice Sheet (WAIS) Divide Project Members*, 2015]. We now examine the pervasive, higher frequency signals of the WD continuous CH_4 record to further advance our understanding of natural methane variability.

2. Materials and Methods

2.1. WAIS Divide Continuous CH_4 Data

For this study it is important to highlight the precision and resolution WD continuous CH_4 measurements (Table 1) (for further details, see Table S1 in the supporting information [*Rhodes et al*., 2015]). Measurements are reproducible to within ±1.5–4.2 ppb and each experiment time-integrated data point has an internal precision of ±0.4–1.4 ppb (2σ). Mean sampling resolution, which is dictated by the optimal integration time used in data processing, varies from 0.4 to 1.1 years depending on the analytical setup and the depth/age range being sampled in the ice core. Mixing and diffusion of the gas sample within the analytical system causes some signal smoothing and gives rise to a limit of resolution (shortest resolvable scale) that varies between 0.5 and 12.6 years, again dependent upon the analytical setup and the ice core depth/age (Table 1).

In practice, the temporal resolution of the WD continuous atmospheric CH_4 record is governed by the temporal resolution of the ice core gas archive itself; diffusive mixing within the firn column and the gradual occlusion of air bubbles cause smoothing of the atmospheric signal and effective removal of high-frequency signals such as the seasonal cycle [*Schwander et al*., 1997]. At WD this effect is minimal in comparison to other Antarctic ice cores because accumulation rates are relatively high (22 cm ice yr^{-1} present day and 10 cm ice yr^{-1} Last Glacial Maximum (LGM) [*Buizert et al*., 2015]). However, estimated gas age distribution widths (full width at half maximum (FWHM)) at the base of the firn for this interval in WD range from 20 to 57 years (Table 2), so the effects of firn smoothing must still be considered if we attempt to examine centennial-scale features (section 3.2.3). For the WD record, the degree of smoothing resulting from firn-based processes always exceeds that resulting from the analytical system, possibly excepting gas ages >60 ka B.P. [*Rhodes et al*., 2015].

In order to fill data gaps, reduce noise, and obtain an even time step, a cubic smoothing spline was fitted to the experiment-time-integrated WD CH_4 measurements by *Rhodes et al*. [2015]. We continue to utilize this

Table 1. Resolution and Precision of WD Continuous CH_4 Measurements Made With Three Different Laser Spectrometers Over Two Analytical Campaigns[a]

		Year		
Instrument	Units	2012 Picarro CFADS36	2013 Picarro G2401	2013 SARA
Optimal integration time	(s)	20	20	5
	(year)	0.4 (0.2–0.7)	1.1 (0.5–3.0)	0.6 (0.2–1.1)
Shortest resolvable scale[b]	(cm)	5.5	6.2	5.4
	(year)	1.2 (0.5–2.0)	3.7 (1.7–10.1)	6.3 (1.4–12.6)
System response time (t_{10-90})[c]	(s)	104	138	121
	(year)	2.1 (0.8–3.4)	7.6 (3.4–20.5)	13.6 (3.0–26.0)
Internal precision (2σ)[d]	(ppb)	1.4	0.4	0.7
Long-term reproducibility[e]	(ppb)	2.8	1.5	4.2
Age range analyzed	(ka, WD2014)	9.819–23.631	26.715–26.987	26.362–26.715
			27.596–45.532	26.987–27.596
			52.841–60.354	45.532–52.841
				60.354–67.344

[a]Differences may be the result of instrument change or minor alterations to continuous melter and/or gas extraction system. Measurement resolution is expressed as a mean with the range given in parentheses in units of experiment time, depth, and/or gas age.
[b]A periodic signal of this wavelength would be attenuated by 90% at melt rate of 5.5 cm min^{-1}.
[c]Time taken for CH_4 concentration to change between 10 and 90% of total normalized concentration change resulting from switch between two different air standards mixed with degassed water and circulated through the analytical system at gas flow rate of 1.8 mL min^{-1}.
[d]2* Allan deviation at optimal integration time.
[e]Pooled standard deviation between original analyses and replicate stick analyses [see *Rhodes et al*., 2015, Figure S2].

approach here. Experiment-time-integrated data are also displayed in Figures 1 and 2 for reference. The WD2014 time scale and age uncertainties are described by *Sigl et al*. [2016] and *Buizert et al*. [2015].

2.2. Isolating the Centennial-Scale Component

In order to isolate the centennial-scale component of CH_4 variability, we mask the abrupt transitions of Dansgaard-Oeschger (DO) events, which dominate the millennial-scale variability of the Last Glacial Period (Figure 3a). This prevents the generation of signal artifacts, which result from applying Fourier transform-based filters to nonsinusoidal features. The record is first divided into stadial and interstadial periods using

Table 2. Estimates of the Impact of Firn-Based Smoothing on the Atmospheric Trace Gas Record of the WD Ice Core[a]

Gas Age at Midpoint of 5000 Year Window (ka)	Temperature (°C)[b]	Accumulation Rate (cm ice yr^{-1})[c]	Δ Age (year)[c]	FWHM[d] (year)	fA_{100}	fA_{150}	fA_{200}	A_{100} (ice core/atm) (ppb) Δ = 1.5 ppb	A_{150} (ice core/atm) (ppb) Δ = 3 ppb
12.32	−31.4	22.3	215	20	0.67	0.78	0.84	10/15	15/19
17.32	−38.0	12.6	423	31	0.52	0.66	0.74	4/8	7/11
22.32	−40.8	11.2	496	58	0.24	0.45	0.57	4/19	8/18
27.32	−38.6	12.6	416	36	0.45	0.62	0.71	7/15	15/24
32.32	−38.3	11.4	438	36	0.44	0.61	0.70	6/13	10/16
37.32	−37.2	15.6	349	28	0.57	0.70	0.77	7/13	9/13
42.32	−37.7	16.0	347	35	0.48	0.65	0.73	9/18	11/17
47.32	−36.8	18.5	305	30	0.55	0.69	0.77	10/19	12/17
52.32	−35.9	18.3	296	32	0.52	0.67	0.76	9/17	11/17
57.32	−35.8	18.1	297	36	0.47	0.64	0.74	9/20	10/16
62.32	−37.2	17.5	324	41	0.41	0.60	0.71	9/21	12/20

[a]"Firn filters" were produced for each gas age window by using temperature and accumulation values shown by using the OSU firn air transport model [*Rosen et al*., 2014]. fA_{100} denotes the fraction of the amplitude of a 100 year wavelength periodic signal *remaining* after applying the filter. Left-hand A_{100} value is the median peak-to-peak signal amplitude identified in the ice core for that time window by using Δ = 1.5 ppb in peak detection code (Figure 3c). Right-hand A_{100} value is an estimate of the original peak-to-peak amplitude of the atmospheric signal prior to firn smoothing. A_{150} values are the equivalent for a 150 year wavelength signal identified by using Δ = 3 ppb.
[b]*Cuffey et al*. [2016].
[c]*Buizert et al*. [2015].
[d]Full width at half maximum (FWHM) is a measure of the gas age distribution spread in the closed porosity at the close-off depth (where no open porosity remains). Higher values indicate more mixing of the atmospheric signal over time in the firn pack and stronger damping of high-frequency signals.

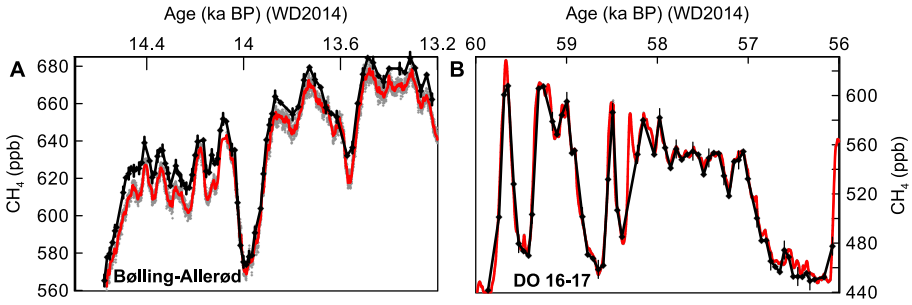

Figure 1. Centennial-scale variability in WD continuous CH_4 record replicated by discrete measurements. Experiment-time-integrated data (gray) and 2 year spline fit (red) are shown. (a) CH_4 variability through the Bølling-Allerød. Discrete WD CH_4 measurements performed at Oregon State University (black symbols, uncertainty bars 3.1 ppb 2σ) [*Marcott et al.*, 2014]. (b) CH_4 variability across DO 16-17. Discrete WD CH_4 measurements performed at Pennsylvania State University (black symbols, uncertainty bars 7.3 ppb 1σ (replicate samples contiguous in depth)) [*WAIS Divide Project Members*, 2015].

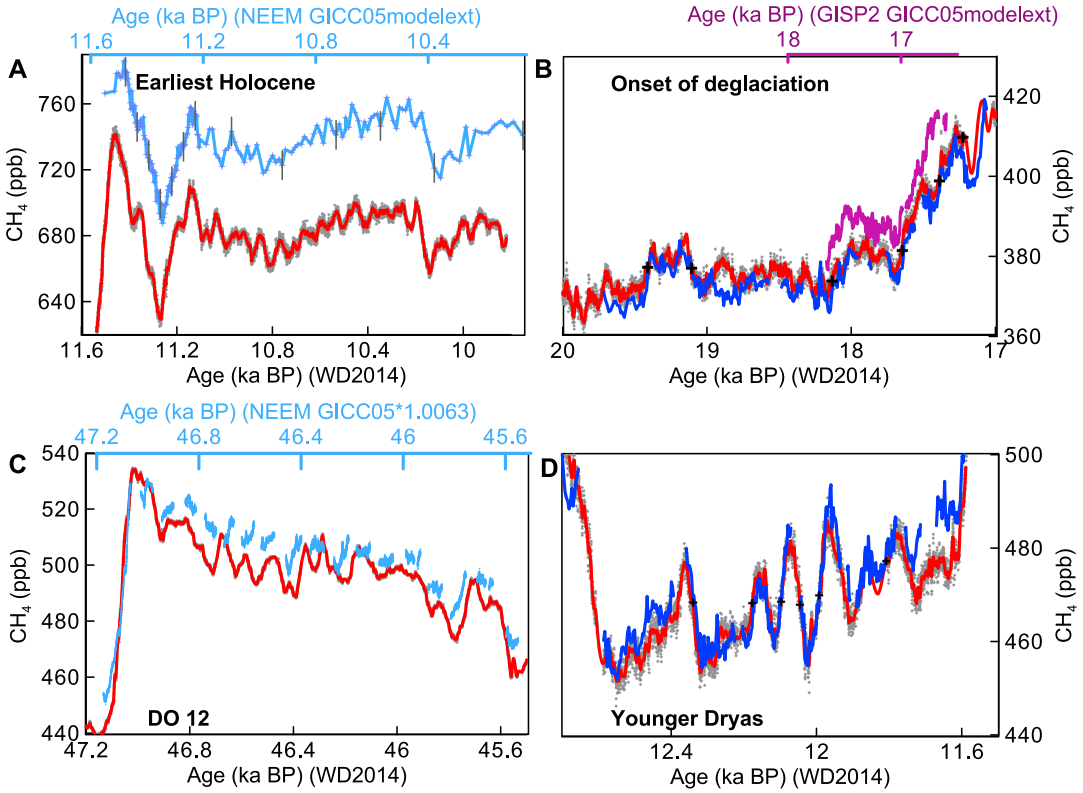

Figure 2. WD continuous CH_4 record compared to other ice core CH_4 records. WD experiment-time-integrated data (gray) and 2 year spline fit (red) are shown. (a) Earliest Holocene in WD CH_4 and NEEM discrete measurements (gray crosses and pale blue line). (b) Initiation of deglacial CH_4 rise in WD compared to GISP2 continuous data (purple) and Fletcher Promontory (Antarctica) continuous data (dark blue). (c) WD CH_4 across DO12 compared to NEEM CH_4 record (pale blue) measured using continuous technique [*Chappellaz et al.*, 2013]. NEEM CH_4 values are reduced by 20 ppb CH_4 to aid viewing. (d) CH_4 variability within the Younger Dryas resolved in WD and Fletcher Promontory (dark blue) records. Fletcher Promontory data have been transferred to the WD2014 time scale using tie points shown (black crosses). NEEM and GISP2 data are plotted on the GICC05modelext time scale [*Rasmussen et al.*, 2013; *Seierstad et al.*, 2014], which is multiplied by 1.0063 in Figure 2c to translate age to WD2014. Where data from different ice cores are plotted on the same panel, the two *x* axes may be offset to aid viewing. This alignment of age scales indicates that WD2014 and NEEM GICC05modelext gas ages are offset by 132 years at the preboreal oscillation CH_4 minimum (Figure 2a) and that WD2014 and GISP2 GICC05modelext gas ages are offset by ~600 years at the initial CH_4 deglacial increase (Figure 2b).

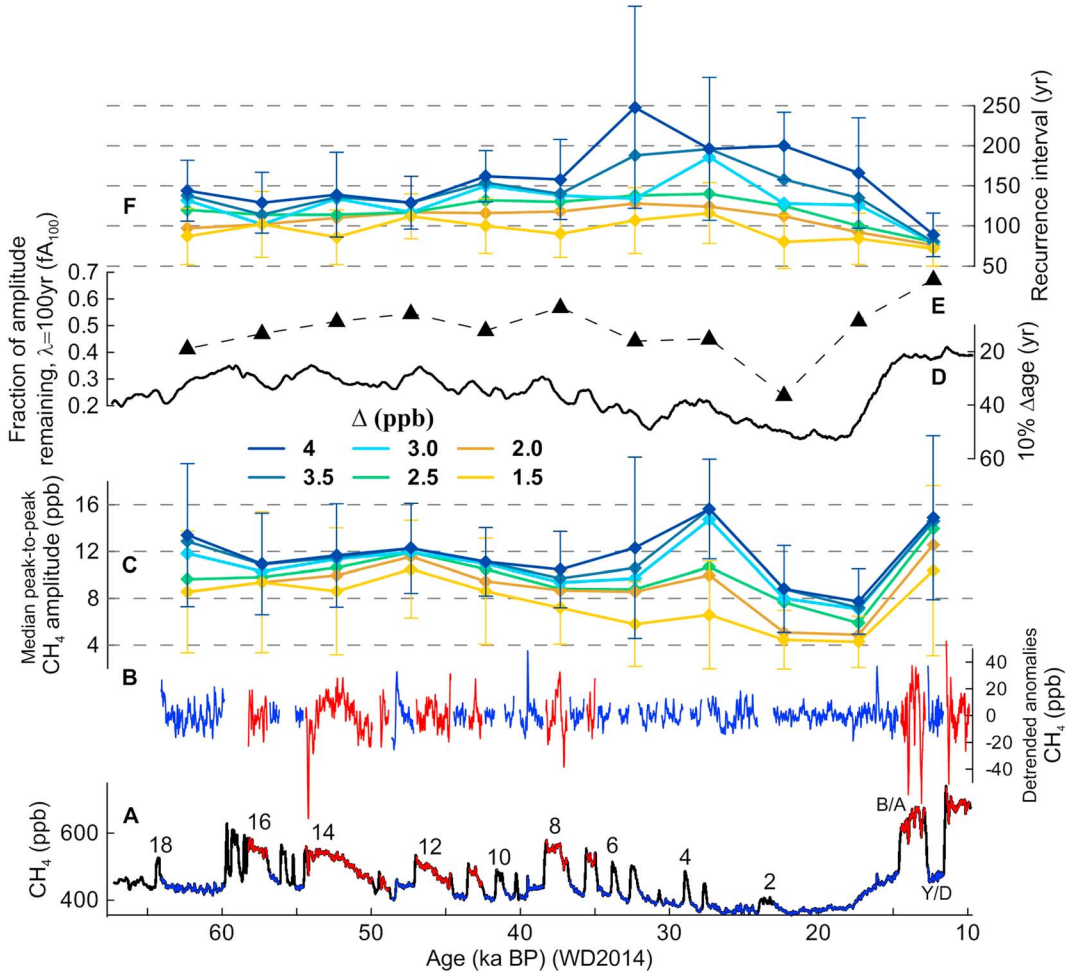

Figure 3. Recurrence intervals and amplitude of the centennial component of WD CH_4 variability. (a) WD CH_4 2 year spline (black) divided into interstadial (red) and stadial (blue) periods. (b) Detrended CH_4 anomalies after removal of ±50 years either side of each stadial-interstadial transition and exclusion of periods <300 year duration. (c) Median peak-to-peak amplitude of CH_4 centennial component (red and blue in Figure 3a) for 5000 year duration nonoverlapping windows (points plotted at center of window). The results obtained using different Δ values (section 2.3.1) are color coded as indicated by legend. Uncertainty bars (for Δ values of 4 and 1.5 ppb only) denote the median absolute deviation; (d) 10% of the gas age-ice age difference (Δage) through the WD ice core, intended to give a rough indication of the change in firn-based smoothing effect though time, with larger values suggesting more smoothing of the atmospheric gas record. The values should be read from the right-hand axis, which is inverted. (e) Fraction of the amplitude (fA) of a periodic atmospheric signal with 100 year wavelength (λ) that would be preserved in the WD ice core after smoothing of the gas record by firn-based processes, as predicted by the Oregon State University firn air model (black triangles, see also Table 2). (f) As in Figure 3c but for median recurrence interval.

the transition midpoint ages provided by *Buizert et al*. [2015]. At each transition midpoint, 50 years of data are removed from either side. Any remaining stadial or interstadial period <300 year duration is removed from analysis. Each individual period is then linearly detrended and its mean is subtracted to generate anomalies that characterize the centennial-scale component of the CH_4 record (Figure 3b).

2.3. Characterizing the Centennial-Scale Component

Two different methods are used to characterize the centennial-scale CH_4 variability.

2.3.1. Peak Detection

First, we utilize a simple Matlab peak detection algorithm designed to pick data maxima and minima. It requires a threshold value (Δ) to be specified. A data point is considered a maximum if it has the maximal value and was preceded by a minimum value lower by Δ (Figure S1). The peak detection algorithm is applied to the CH_4 record after DO event transitions have been removed (red and blue lines in Figure 3a). We test Δ

values of 1.5–4 ppb, equivalent to the long-term reproducibility of the data (Table 1). We additionally specify a minimum time interval between adjacent maxima and minima of 25 years (equivalent to 50 year signal wavelength) because it is highly unlikely that a higher frequency signal could survive the smoothing action of firn-based processes (see FWHM, Table 2). Once the maxima and minima of adjacent peaks have been identified, recurrence intervals and peak-to-peak amplitudes are calculated. Median recurrence intervals and peak-to-peak amplitudes are calculated for 5000 year duration, nonoverlapping time windows.

2.3.2. Time Series Analysis

Second, we employ spectral analysis using the freely available REDFIT software [*Schulz and Mudelsee*, 2002]. REDFIT uses the Lomb-Scargle method that is suitable for data with gaps. We apply REDFIT to the WD CH_4 anomalies (Figure 3b) from 67.2 to 27 ka B.P. to avoid the effects of time-varying firn smoothing on the centennial-scale signal amplitudes (see section 3.2.3). The average sample interval is 2.62 years, and analysis is performed using Welch spectral windows, an oversampling factor of 15, and 3 overlapping windows. A "hifac" value of 0.102 is used to set the highest frequency analyzed to 0.0195 years (51 year wavelength). To assess the significance of spectral peaks, confidence levels were produced by fitting 1000 Monte Carlo simulations of autoregressive (AR(1)) red noise to the data and calculating power spectra for each. The 90% and 95% quantiles of all the AR(1) power spectra are used as confidence levels.

3. Results

3.1. High-Frequency Variability: Climate or Artifact?

Figure 1 shows two examples of the novel centennial-scale variability resolved within the WD continuous CH_4 record plotted with discrete CH_4 measurements made on the same ice core. The submillennial-scale variability of the continuous CH_4 data, particularly the amplitude and wavelength of the signals, is reproduced extremely well by the discrete data throughout the record, confirming that it is a reproducible feature of the WD ice core gas archive. Despite the relatively high resolution (1–3 m or 15–80 years) of the discrete data, some of this signal may have been dismissed as analytical or archival noise without the incredibly detailed continuous CH_4 information.

To ascertain whether or not this new variability is unique to WD, we compare WD continuous CH_4 to other CH_4 data available at comparably high resolution (Figures 2a–2d). Discrete measurements on the North Greenland Eemian (NEEM) ice core from the earliest Holocene faithfully reproduce the variability observed in the WD record (Figure 2a). The full amplitude of the preboreal oscillation at 11.3 ka (WD2014) is captured along with small variations in CH_4 concentration during the sharp transitions toward and away from the CH_4 minimum. Furthermore, the broad trough centered at 10.7 ka (WD2014) and abrupt decrease at 10.2 ka are reproduced, together with quasi-centennial-scale oscillations superimposed on the record.

In another example, a 24 m section of CH_4 data from the Greenland Ice Sheet Project 2 (GISP2) ice core, analyzed using our continuous-flow system, reproduces the onset of the deglacial CH_4 rise at 17.7 ka and captures some of the centennial-scale oscillations in CH_4 shown in the WD continuous record (Figure 2b), most notably between 18.2 and 17.7 ka. The agreement between WD CH_4 and the recently obtained continuous CH_4 record from the Fletcher Promontory (Antarctica) ice core is extremely impressive (Figure 2b). Nearly every centennial-scale feature visible in WD is replicated in the Fletcher Promontory record, the only exception being a short section 19–18.8 ka. This correspondence is all the more remarkable because the same 2650 years of data are contained within just 2 m depth of ice core at Fletcher Promontory, compared to 88 m at WD.

Although the NEEM continuous-flow data set [*Chappellaz et al.*, 2013] CH_4 is relatively noisy and suffers from frequent data gaps, when it is plotted together with WD, it becomes clear that the NEEM record picks up many of the same centennial-scale features across DO12 (Figure 2c). Finally, continuous CH_4 data from the Fletcher Promontory ice core exhibit centennial variability within the Younger Dryas that matches remarkably well with that of the WD record (Figure 2d).

In summary, all the available ice core CH_4 data support the fidelity of the new centennial-scale features we observe in the WD CH_4 record. This indicates that the features represent past variability in global atmospheric methane concentrations and negates the possibility that they are site-specific artifacts resulting from biological in situ production [*Rhodes et al.*, 2013] or layered gas bubble trapping [*Etheridge et al.*, 1992; *Rhodes et al.*, 2016].

3.2. Characterizing the Centennial-Scale CH_4 Variability

3.2.1. The Centennial-Scale Component

The detrended anomalies that comprise the centennial-scale component of the WD CH_4 record exhibit variability that is pervasive throughout the 67.2–9.8 ka record (Figure 3b). By eye, it is possible to see that the nature of the centennial signal changes with time; most notably, the signal amplitude appears reduced around the LGM (Figure 3b). Additionally, the oscillations appear to be the most frequent in the youngest section of the record, the earliest Holocene (Figure 3f). We will explore these observations quantitatively in the following sections.

3.2.2. Recurrence Interval and Signal Amplitude

Peak detection analysis of the centennial-scale component reveals that the WD CH_4 record is characterized by median recurrence intervals of 80–200 years (Figure 3f). The choice of Δ value used in the peak detection algorithm influences the recurrence interval outcome, with lower Δ values leading to shorter recurrence intervals. It is difficult to confidently decide on a Δ value; higher values likely cause some real atmospheric variability to be missed, particularly in regions of the record with relatively strong firn-based signal smoothing (i.e., 35–20 ka; section 3.2.3), while it is also possible that some of the variability identified using a 1.5 ppb Δ value is not paleoatmospheric signal (Figure S1).

However, for most age windows, the median absolute deviations of the recurrence interval estimates (uncertainty bars in Figure 3f) for Δ values of 1.5 ppb and 4 ppb overlap, suggesting that the choice of Δ value does not produce a significant bias. It is only in the data window centered on 22.32 ka that the two estimates differ significantly, with a median recurrence interval of 80 years estimated using $\Delta = 1.5$ ppb and a median recurrence interval of 200 years estimated using 4 ppb. The range of recurrence interval durations with different Δ values is smallest for the age window encompassing the earliest Holocene, for which all Δ values suggest a recurrence time of <100 years.

Median peak-to-peak signal amplitudes are typically 8–12 ppb for each 5000 year window between 67 and 35 ka and show no discernible variation with time (Figure 3c). Again, different Δ values produce a range of peak-to-peak amplitude values, but these distributions overlap. Between 25 and 15 ka the peak-to-peak amplitudes are reduced for all Δ values to 4–8 ppb. Amplitudes consistently increase to 10–14 ppb for all Δ values in the 14.82–9.82 ka window of the record.

3.2.3. Damping of Atmospheric Variability in the Firn Column

We now consider to what extent the variations in recurrence time and amplitude with age detailed above may result from damping of the centennial-scale variability by diffusive smoothing of the atmospheric signal in the firn pack. We use a firn air transport model adapted for paleoclimate applications [*Rosen et al*., 2014] to generate filters that simulate the diffusive smoothing of atmospheric signals in the firn for each time window (Table 2). The firn filters are each applied to synthetic time series consisting of sine waves with 100, 150, and 200 year periodicities to assess what fraction of the signal amplitude (fA) remains after firn-based smoothing (Table 2). This exercise suggests that at WD an atmospheric signal of 100 year wavelength would be damped by 33% in the earliest Holocene, 76% around the LGM, and 50% in Marine Isotope Stage (MIS) 3 (Figure 3e). Unsurprisingly, the impact of firn smoothing is most extreme around the LGM when conditions were coldest and driest (Table 2 and Figures 3d and 3e). This is exactly the time period when we observe relatively low-amplitude centennial-scale CH_4 variability. It is therefore possible that the relatively low amplitudes through LGM compared to the Holocene or MIS 3 can be attributed to signal damping by firn-based processes, rather than a real change in the nature of the original atmospheric signal.

The peak detection analysis suggests that recurrence intervals of 80–200 years characterize highest resolvable frequency of the CH_4 record (Figure 3f). If we assume a recurrence time of either 100 or 150 years (roughly equivalent to results using Δ values of 1.5 and 3 ppb, respectively) and use the firn filters generated for WD, then the peak-to-peak amplitudes of each time window can be crudely translated into the original peak-to-peak amplitude of the centennial component of CH_4 atmospheric variability (A_{100} and A_{150}; Table 2). The estimates for both cases are broadly in agreement: an average peak-to-peak amplitude of 16 ppb, with an 8–24 ppb range. The results appear to indicate that signal amplitudes in the 19.82–14.82 ka window are lower than the others even after correction for firn smoothing. While this may be possible, it is likely that the rapid changes in temperature and accumulation over this window cause the firn smoothing effect to be

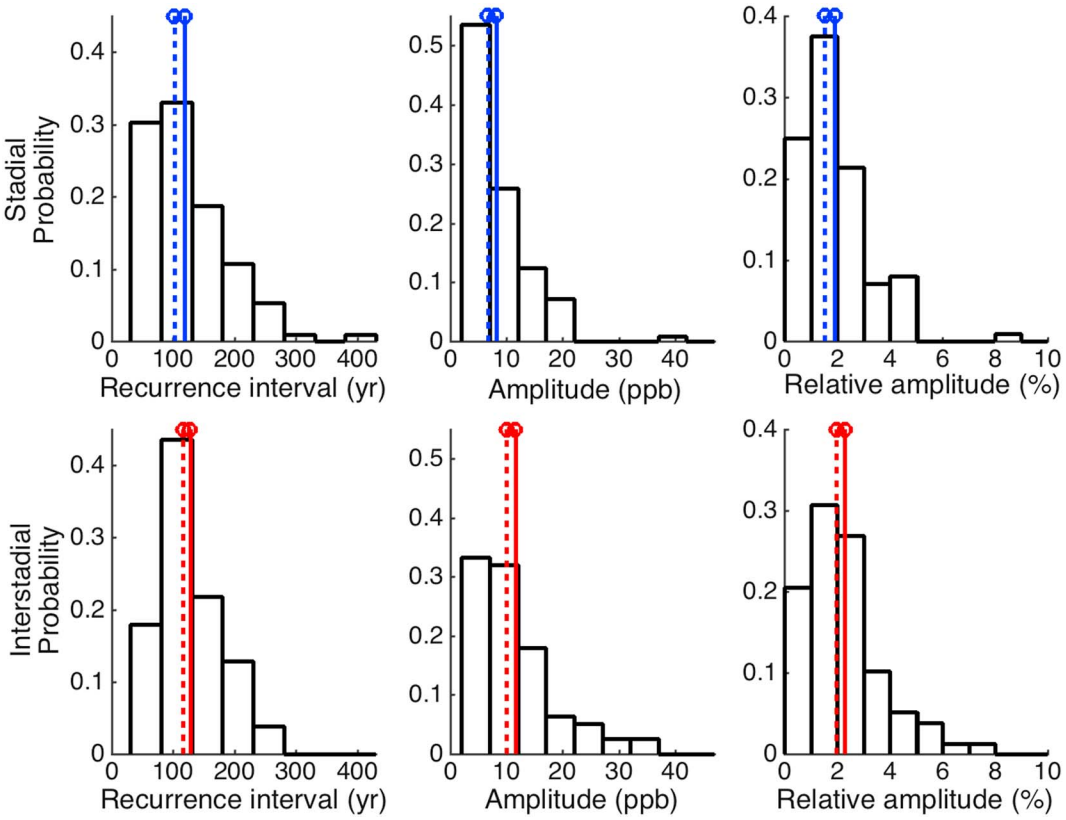

Figure 4. Probability distributions of the recurrence intervals and peak-to-peak amplitudes identified for the centennial-scale component of WD CH_4 record (DO events 3–18 only). (top row) Stadial ($n = 112$) and (bottom row) interstadial ($n = 79$) probability distributions are compared. Relative amplitude (Figure 4, right column) is the peak-to-peak amplitude of the centennial-scale signal relative to the long-term CH_4 background concentration (300 year running median). A Δ value of 2 ppb was used in peak detection code. Population mean values (solid lines) and median values (dashed lines) are indicated on each histogram.

underestimated. Overall, once potential firn smoothing is taken into account, there is no significant difference between the peak-to-peak amplitudes of the recurring 80–200 year signal between the Holocene and Last Glacial Period. Additional, ultrahigh-resolution CH_4 records are needed to verify this result because the estimation of the firn smoothing effect is highly uncertain.

3.2.4. Comparison Between Stadials and Interstadials

We now focus on the WD CH_4 record between 67.2 and 27 ka (DO events 3–18 only) to investigate whether centennial-scale CH_4 variability has the same characteristics in stadial versus interstadial periods. We take the recurrence intervals and peak-to-peak amplitudes produced by the peak detection analysis and bin them into stadial and interstadial periods. Probability distributions for the recurrence intervals in stadial and interstadial periods are similar (Figure 4). The median recurrence interval is 102 years in stadial periods and 116 years in interstadial periods. In contrast, the probability distributions for signal peak-to-peak amplitude are quite different for stadials versus interstadials; stadials are much more likely to have low-amplitude signals (<7 ppb, mean = 8 ppb), while interstadials are more likely to have relatively large (>17 ppb, mean = 12 ppb) amplitude signals (Figure 4). A Welch's two-sample *t* test, assuming unequal variances, indicates that the interstadial and stadial mean amplitudes are significantly different (5% significance level, for $\Delta = 2$ ppb). However, if the peak-to-peak amplitudes are normalized to the underlying mean stadial or interstadial CH_4 concentration to calculate a relative amplitude, then the interstadial and stadial probability distributions appear similar and their mean values are not significantly different (Figure 4). These two results (significant difference for absolute amplitudes but not relative amplitudes) hold true for all Δ values tested. This suggests that the amplitude of the centennial component varies in proportion to the longer-term CH_4 background changes related to DO events.

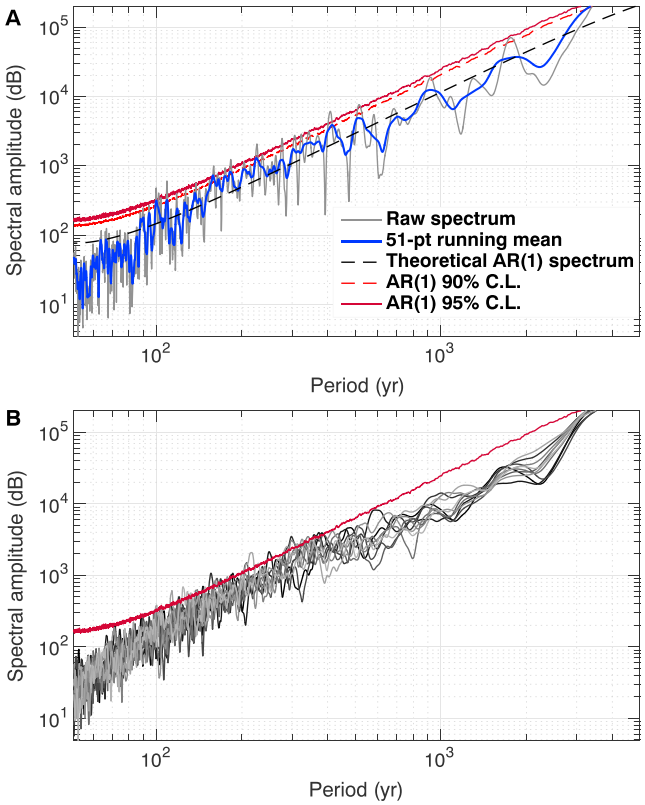

Figure 5. (a) Lomb-Scargle power spectrum of the WD CH_4 edge-masked, detrended anomalies (from Figure 3b) from 67.2 to 27 ka only (gray line) and a 51-point running mean of that power spectrum (blue line). The 90% and 95% confidence levels (CLs) (red lines) are the 90th and 95th quantiles of 1000 Monte Carlo-generated autoregressive noise (AR(1)) model spectra. The 50% quantile is also shown (dashed black line). Spectral peaks in the WD CH_4 power spectra must exceed the 90% or 95% confidence levels for them to be significantly different to purely red noise features. The 6 dB bandwidth is 8.77e−5. (b) Ten 51-point smoothed power spectra of the same WD CH_4 data but with the WD2014 gas ages modified within 2σ uncertainties (gray lines). The 95% confidence level is also shown (red line).

It is important to note that the difference between stadial and interstadial signal amplitudes cannot be related to the differences in the degree of firn-based smoothing. WD is an Antarctic ice core so accumulation rate and temperature at the site vary in step with Antarctic Isotope Maxima, not DO events [*Buizert et al.*, 2015]. If we were studying a CH_4 record from a Greenland ice core, then we would be concerned that the twofold increases in accumulation rate [*Rasmussen et al.*, 2013] and 5–16.5°C temperature swings [*Kindler et al.*, 2014] across DO events would cause significant changes in signal damping in the firn pack.

3.2.5. Spectral Information

The Lomb-Scargle periodogram of the 67.2–27 ka portion of the CH_4 record (Figure 5a) exhibits some significant spectral peaks at 95% confidence level, but these peaks are very narrow. If the spectrum is smoothed, then only peaks between 100 and 300 year periods are significant. This result is broadly consistent with the findings of the peak detection method.

Despite this apparent significant periodicity to the signal, we are cautious in our interpretation of this result due to the age uncertainty associated with the WD2014 age scale. For the majority of the 67.2–27 ka record, mean gas age uncertainty is 390 years (2σ), which is of course of the same order as the periodicities we are attempting to isolate. To test the influence of age uncertainty on the Lomb-Scargle spectral analysis, we construct 10 synthetic WD2014 age scales by allowing the gas age to randomly vary within the age uncertainties while maintaining stratigraphic order. The resulting 10 power spectra display significant periodicities within a 100–500 year range (Figure 5b). The significant periodicities differ between the 10 synthetic spectra and also differ from those of the original data set (Figure 5). Therefore, we conclude that we cannot rule out the presence of significant periodicity in centennial-scale CH_4 variability, but we equally cannot identify potential periodicity to better than a broad 100–500 year range, given the associated age uncertainties.

4. Discussion

4.1. Origin of Centennial-Scale CH_4 Variability

We have identified a previously undetected mode of natural CH_4 variability in the WD continuous CH_4 record (67.2–9.8 ka). Our analysis indicates that the magnitude of CH_4 variability within stadial versus interstadial periods scales in proportion to the underlying CH_4 concentration (Figure 4), which changes by up to 260 ppb between stadial and interstadial levels. Uncertainty on the degree of signal damping exerted by firn-based processes in the Last Glacial compared to the Early Holocene prevents us from reaching any similar conclusion about the relative amplitude of CH_4 variability between the glacial and interglacial. As a result, our

Table 3. Estimated Changes in CH_4 Source or Sink Strength Responsible for Centennial-Scale CH_4 Signals in Stadial and Interstadial Periods[a]

				Source Change		Sink Change	
	Mean p2p Amplitude in Ice Core (ppb)	Mean p2p Amplitude in Atmosphere (ppb)	Long-Term CH_4 Concentration (ppb)	τCH_4 (year)	$\Delta CH_{4\ emis}$ (Tg yr^{-1})	Constant $CH_{4\ emis}$ (Tg yr^{-1})	$\Delta\tau CH_4$ (year)
Stadial	8	17	420	8.5	6.0	170	0.3
Interstadial	12	24	509	8.3	9.1	176	0.4

[a]Calculations assume that the signal wavelength is uniformly 100 years. Peak-to-peak (p2p) amplitudes observed in the ice core are crudely corrected for firn-based signal damping of $fA_{100} = 0.49$ (mean value for 24.82–64.82 ka; Table 2).

discussion of source or sink change attribution focuses on the centennial-scale CH_4 variability 67.2–27 ka, across the major DO events of MIS 3.

The sub-DO event centennial-scale atmospheric CH_4 variability must result from an imbalance of CH_4 emissions and CH_4 removal. The typical peak-to-peak amplitude of this CH_4 variability (17 ppb in stadials and 24 ppb in interstadials corrected for firn smoothing using a firn air transport model; section 3.2.3) is only about half the modern-day CH_4 seasonal cycle at the South Pole (https://www.esrl.noaa.gov/gmd/)—a fraction of that associated with the transition from the Last Glacial to Holocene (~320 ppb) or stadial to interstadial transitions (50–260 ppb).

The CH_4 atmospheric burden (B) varies between 1020 and 1780 Tg across the major DO events of MIS 3. The magnitude of change in CH_4 emissions ($CH_{4\ emis}$) or sink strength (CH_4 lifetime = τCH_4) required to produce an observed change in B can be calculated by rearranging equation (1).

$$dB/dt = CH_{4\ emis} - B/\tau CH_4 \quad (1)$$

For 67.2–27 ka, $CH_{4\ emis}$ varies between 135 and 210 Tg yr^{-1} and the increase in CH_4 emissions ($\Delta CH_{4\ emis}$) at the onset of major DO events, such as DO 17, exceeds 50 Tg yr^{-1}. To roughly estimate the CH_4 emissions change required to produce the smaller centennial-scale variability, we consider stadials and interstadials separately, using mean signal amplitudes that have been corrected to the same degree for the damping effect of firn-based smoothing (Table 3) and a uniform signal wavelength of 100 years in both cases. Slightly different τCH_4 values are used for stadial and interstadial periods (Table 3) following *Levine et al.* [2012], but this makes a negligible difference to the result.

The estimated $\Delta CH_{4\ emis}$ is 6.0 Tg yr^{-1} in stadials and 9.1 Tg yr^{-1} in interstadials (Table 3). This is about half the global CH_4 emissions' increase between 2005 and 2010 (15–20 Tg yr^{-1} [*Nisbet et al.*, 2014]), but an order of magnitude lower than the estimated emissions changes at onset of major DO events.

4.1.1. Sink Change?

The sink strength change ($\Delta\tau CH_4$) required to generate the centennial-scale CH_4 variability observed is estimated by holding the $CH_{4\ emis}$ term in equation (1) constant. For the idealized stadial period, a 0.3 year change in τCH_4 is required, while a 0.4 year change is required in the interstadial scenario. These values appear small; they equate to a 4.0 or 4.9% increase in τCH_4 over 50 years, but could such changes in τCH_4 occur on centennial time scales?

Modeling studies suggest that the CH_4 removal rate remained constant across both glacial-interglacial [*Levine et al.*, 2011; *Murray et al.*, 2014] and stadial-interstadial transitions [*Levine et al.*, 2012]. *Levine et al.* [2011, 2012] attribute this to a balance between two opposing processes: (1) the control of OH production by humidity, which is closely related to air temperature, and (2) emissions of nonmethane volatile organic compounds (NMVOCs) that promote OH removal, which are also partly controlled by air temperature. As *Levine et al.* [2011] outline, at the LGM, lower air temperature and decreased humidity resulted in less OH production, but this was offset by reduced NMVOC emissions from plants that in turn caused less OH to be removed from the troposphere. This implies that τCH_4 is sensitive to tropical air temperatures—the majority of tropospheric OH is located at tropical latitudes and so most oxidation of CH_4 also occurs there [*Crutzen and Zimmermann*, 1991]. *Levine et al.* [2012] report that the promotion of OH production by higher humidity has a slightly greater influence than the opposing process so that a warming event actually leads to a small net decrease in τCH_4. In their model, a 2.6% reduction in τCH_4 occurs across an idealized stadial-interstadial transition, equivalent to a 9 ppb reduction in atmospheric CH_4 concentration [*Levine et al.*, 2012]. The

temperature change at the tropics is 1°C in this simulation. If the sensitivity of τCH_4 to climatic change, in particular to tropical temperatures, is correct in *Levine et al.*'s model, then their results suggest that for a sink change to be solely responsible for the 7–24 ppb CH_4 oscillations within stadial and interstadial periods, repeated tropical air temperature fluctuations on the order of 1°C would be required at centennial time scales. Reconstructions over the last 400 years suggest that tropical SSTs in individual basins varied on multidecadal (20–80 years) time scales by $<$0.5°C [*Tierney et al.*, 2015, Figure 10].

4.1.2. Source Change?

Having largely ruled out a change in sink strength as the mechanism behind the centennial CH_4 variability, we now assess the three major CH_4 sources that could be responsible for the estimated 6–9.1 Tg yr^{-1} fluctuations in CH_4 emissions: boreal wetlands (or peatlands), tropical wetlands, and biomass burning.

Of the major CH_4 sources, boreal wetlands are the least likely to be responsible for the relatively constant centennial CH_4 variability throughout the record because their ability to produce CH_4 was severely reduced during the Last Glacial due to the cold temperatures and expanded Northern Hemisphere ice sheets [*Kaplan*, 2002].

While tropical wetland emissions did also change substantially across DO events [*Brook et al.*, 2000; *Hopcroft et al.*, 2011; *Sperlich et al.*, 2015], it is conceivable that a different mode of shorter time scale variability could operate concurrently—akin to the decadal-scale variations in CH_4 growth rate superimposed on long-term CH_4 increase in the instrumental period [*Dlugokencky et al.*, 2009; *Nisbet et al.*, 2016; *Schaefer et al.*, 2016]. It is generally accepted that an atmospheric teleconnection between the high northern latitudes and the tropics caused relatively warm, wet interstadial periods in the tropics and subtropics with relatively high tropical wetland CH_4 emissions, and vice versa during stadial periods [*Brook et al.*, 2000; *Chiang and Bitz*, 2005]. This teleconnection explains the tight coupling between Greenland ice core $\delta^{18}O$, (sub-)tropical climate archives, and CH_4 across DO events (Figure 6). When WD CH_4 and Greenland ice core $\delta^{18}O$ are compared at the centennial scale, two categories of centennial-scale feature are common to both: (1) many interstadial periods begin with a short duration (~100 years) CH_4 peak that reaches the highest concentration within that period, and analogous features are identifiable in Greenland $\delta^{18}O$ (yellow shading, Figure 6); (2) several DO events display an abrupt rebound event just prior to a sharp decrease to stadial levels. As noted and exploited by *Buizert et al.* [2015] for the purposes of ice core synchronization, these events are also identifiable in Greenland $\delta^{18}O$ (green shading, Figure 6). In addition, we argue that some of the rebound events mentioned above are identifiable in the Cariaco and Arabian Sea sediment reflectance records and also in some highly resolved sections of the Bermuda Rise SST reconstruction (Figure 6). This apparent coincidence of centennial-scale features in CH_4, Greenland ice core $\delta^{18}O$ and (sub-)tropical proxy archives suggests that a similar high-latitude tropical teleconnection to that operating across DO events is responsible for the two categories of centennial-scale feature identified, with variations tropical wetland emissions causing the CH_4 signal.

However, other variability in CH_4 and Greenland ice core $\delta^{18}O$ within stadial or interstadial periods shows little correspondence at centennial time scales (Figure 6). Cross-wavelet analysis indicates that the two records are only sporadically coherent at centennial periods (Figure S2). This mismatch may be due to inaccuracies in the time scales of both records, but, visually at least, it is difficult to conclude that the two signals are coherent at centennial time scales, except across the features mentioned above. Perhaps a high-latitude tropical teleconnection is not responsible for all the CH_4 variability, or Greenland ice core $\delta^{18}O$ does not faithfully record such variability at centennial time scales.

In comparison to tropical wetlands, biomass burning is a small source of CH_4 emissions in the Last Glacial [*Möller et al.*, 2013] but one capable of responding rapidly to climatic change [*Daniau et al.*, 2010; *Fischer et al.*, 2015]. If tropical climate did vary on centennial time scales during the Last Glacial, then it is likely that biomass burning emissions, as well as tropical wetland emissions, would have responded to this. Investigation of high-resolution ice core black carbon and ammonium records holds some promise for reconstructing region fire frequency at these time scales [*Bisiaux et al.*, 2012; *Fischer et al.*, 2015]. Additionally, the $\delta^{13}CH_4$ signature of tropical wetland CH_4 ($-$55‰ [*Dlugokencky et al.*, 2011]) is significantly different from that of C4 plant species in tropical grasslands that are vulnerable to biomass burning ($-$17‰ [*Dlugokencky et al.*, 2011]), potentially allowing reconstruction of relative changes in source strength.

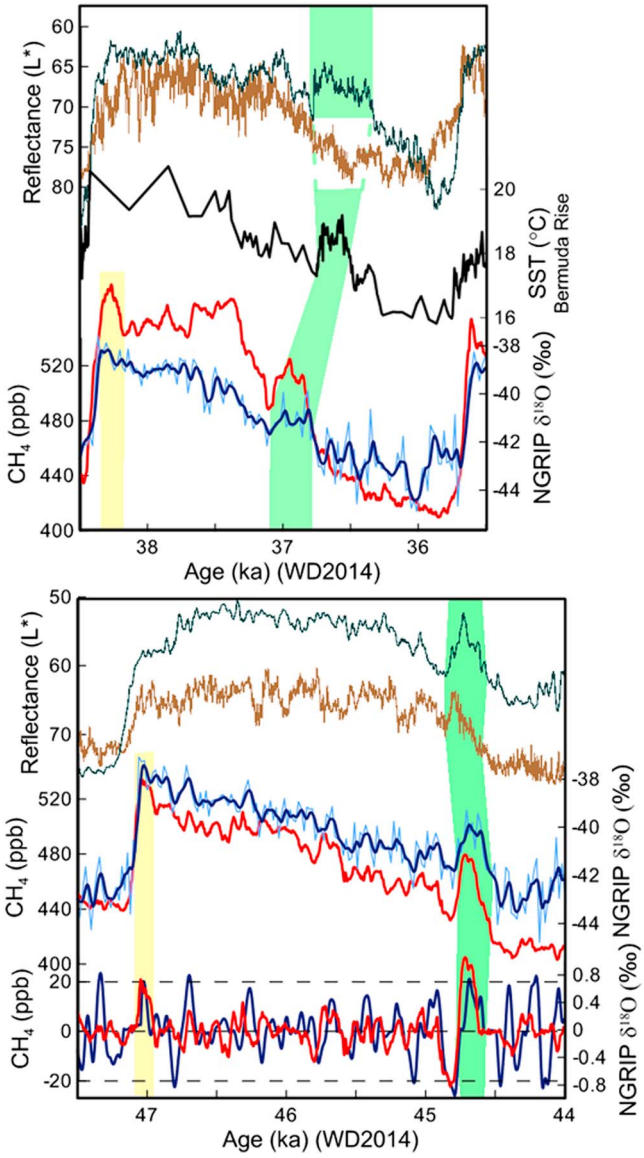

Figure 6. WD CH_4 compared to other high-resolution records of paleoclimate across (top) DO8 and (bottom) DO12. All records have been transferred to the WD2014 age scale. WD CH_4 (red) is plotted with no lag relative to NGRIP $\delta^{18}O$ (blue lines); i.e., age is WD2014 age + 25 years. A filter representing smoothing-action of firn-based processes at WD during MIS3 (Table 2) has been applied to NGRIP $\delta^{18}O$ 20 year mean data (light blue) to generate a version of NGRIP $\delta^{18}O$ with comparable smoothing to WD CH_4 (dark blue). Cariaco basin (light brown, 50-point running median) and Arabian Sea (dark green, 50-point running median) sediment core reflectance data [*Deplazes et al.*, 2013] and alkenone-derived sea surface temperatures from Bermuda Rise (black) [*Sachs and Lehman*, 1999] show some similar sub-DO event features (green shading). The isolated centennial-scale variability of the WD CH_4 and firn-smoothed NGRIP $\delta^{18}O$ records are shown in Figure 6 (bottom).

Constraints on possible CH_4 source contributions might be gained by calculating the interpolar difference at centennial-scale resolution, but no Greenland ice core CH_4 record of equivalent quality (precision and temporal resolution) is available at present and careful consideration of the firn-based smoothing would be required.

4.2. Possible Mechanisms Behind CH_4 Variability

At present, our understanding of possible source changes is limited by the lack of other comparable resolution paleoarchives. However, we present a working hypothesis to stimulate future investigation. We

propose that the centennial-scale CH_4 signal represents variability in low-latitude climate, i.e., oscillation between warmer, wetter conditions and drier, cooler conditions, and that this variability leads to small changes (~6–9.1 Tg yr^{-1}) in cumulative emissions from tropical wetlands and biomass burning. We offer three suggestions as to the possible driving mechanism behind our hypothesized variability in low-latitude climate, in no particular order:

1. The *Atlantic Multi-decadal Oscillation* (AMO) results in variability in North Atlantic sea surface temperatures over 65–80 years [*Kerr*, 2000] and has been linked to precipitation variability across the Sahel [*Zhang and Delworth*, 2006] and the Indian monsoon region [*Goswami et al*., 2006]. This mechanism would cause teleconnection between the North Atlantic and the tropics, which we find only limited evidence for at centennial time scales in the paleoclimate archives.
2. *Solar activity* has been linked to various sea surface temperature and precipitation regimes over many time scales [*Gray et al*., 2010, and references therein]. For example, *Neff et al*. [2001] found a good correlation between the radiogenic isotope ^{14}C record from tree rings and a speleothem $\delta^{18}O$ record from Oman, linking solar activity to monsoon intensity. The 80–90 year and the 208 year solar cycles (Gleissberg and De Vries) are within the range of the recurrence intervals identified in WD CH_4 variability, but we are not able to confirm whether the CH_4 variability is periodic in nature, as would be required by solar forcing.
3. Centennial-scale variability in tropical hydroclimate could be internal variability linked to the *El Niño–Southern Oscillation* (ENSO) and the related *Pacific Decadal Oscillation* (PDO). Although ENSO typically recurs at a 2–7 year interval, century-scale changes in signal variability have been identified in the Holocene [*Cobb et al*., 2013]. Furthermore, ENSO has been shown to influence the interannual variability in tropical wetland methane emissions [*Hodson et al*., 2011] and biomass burning [*van der Werf et al*., 2006]. Recent work has also suggested that a combination of ENSO and AMO can explain much of the variability in continental precipitation over the last century [*García-García and Ummenhofer*, 2015]. We note that relatively little is known about ENSO variability or teleconnections in glacial periods and that both may have differed from Holocene conditions [*Ford et al*., 2015; *Merkel et al*., 2010].

4.3. Links to Late Holocene CH_4 Variability

The new mode of natural CH_4 variability we identify in the WD ice core may be related to the subcentennial features resolved in late Holocene ice core CH_4 records [e.g., *Mitchell et al*., 2011]. Applying the simple peak detection algorithm used earlier (section 2.3.1) to late Holocene CH_4 data produces recurrence intervals and signal amplitudes (40–150 years, 10–40 ppb) that are similar to those of the 15–9.8 ka period in the WD record (Table 2).

Although some prominent individual late Holocene CH_4 variations can be linked with reasonable certainty to anthropogenic influences [*Sapart et al*., 2012], the analysis of *Mitchell et al*. [2011], which regressed late Holocene CH_4 against various environmental proxy records, showed the strongest significant correlations ($r = 0.35$, $p < 0.01$) with tropical sea surface temperatures in the Cariaco Basin and with the PDO. Taken together with the similarity of the signal variability, this provides some indication that analogous variability in low-latitude hydroclimate may have persisted through to the late Holocene and even that it could continue to influence the CH_4 budget today [*Nisbet et al*., 2016]. A high temporal resolution, precise CH_4 record that bridges the time gap between the earliest Holocene (9.8 ka) where the WD continuous record terminates and *Mitchell et al*.'s [2013, 2011] late Holocene CH_4 record begins would help to address this issue.

4.4. Potential for Ice Core Gas Record Synchronization

In addition to supplementing our knowledge of natural CH_4 biogeochemistry, the centennial-scale CH_4 signals resolved in the WD ice core provide an excellent target for rapid, precise synchronization of trace gas records between different cores. The CH_4 records can be aligned using centennial-scale features as an age tie point, provided that the other ice core is also from a site with minimal firn-based smoothing of the gas phase. Examples are shown in Figures 2b and 2d, where the CH_4 record from the Fletcher Promontory (Antarctica) ice core is aligned with the WD CH_4 record. In past work, only the onset and termination of the Younger Dryas would have been used as tie points, but here we use six additional tie points to align the records (Figure 2d). The time period between DO2 (23.3 ka) and the Bølling warming (14.7 ka) has proved problematic for aligning discretely measured CH_4 records, but with two data sets measured by continuous

analysis, six age tie points can be identified between 20 ka and 17 ka. Increased precision of time scale alignment will assist future CH_4 IPD studies, age-scale construction, and phasing analysis.

5. Conclusions

The centennial-scale CH_4 variability we observe in the WD ice continuous CH_4 record 67.2–9.8 ka is reproducible and atmospheric in origin. It is also pervasive throughout the record: stadial or interstadial, LGM, or earliest Holocene (Figures 1–3). Our analysis does not identify a significant periodicity to the signal but indicates that recurrence intervals fall within a broad 80–500 year band, with no notable trend over time. Once corrected for the smoothing effect of firn-based processes, signal amplitude is estimated to be 16 ppb (peak-to-peak) on average, with significantly lower absolute amplitudes in stadial periods (17 ppb) relative to interstadial periods (24 ppb). There is no change in signal amplitude relative to the underlying (millennial-scale) CH_4 concentration across DO events.

It is difficult to constrain the origin of this variability without further data (e.g., CH_4 isotopes, improved-quality Greenland CH_4, and additional high-resolution paleoarchives), but we hypothesize that it may be related to tropical climate variability. Other paleoclimate archives show some evidence for tropical hydroclimate variability at analogous time scales. This work raises interesting questions about how the novel CH_4 variability we observe in the Last Glacial and early Holocene may be related to that recorded in late Holocene ice cores and, to some extent, also to atmospheric variability over recent decades.

Acknowledgments

This study was funded by the U.S. National Science Foundation (NSF) grants 0944552, 1142041, and 0968391 to E.J.B. and 0839093 and 1142166 to J.R.M. A European Union Horizon 2020 Marie Curie Individual Fellowship (grant 58120, SEADOG) provided partial support for R.H.R. This work also benefitted from funding to X.F. from the French RPD COCLICO ANR program (ANR-10-RPDOC-002-01), the INSU/LEFE project IceChrono, and the Ars Cuttoli foundation and additionally from the UK Natural Environment Research Council (NERC) grant NE/P009271/1 awarded to L.C.S. Grateful thanks to B. Tournadre for help in Fletcher Promontory ice core analysis. The authors appreciate the support of the WAIS Divide Science Coordination Office at the Desert Research Institute, Reno, NV, USA, and University of New Hampshire, USA, for the collection and distribution of the WD ice core (NSF grants 0230396, 0440817, 0944348, and 0944266). We are grateful to all participants in the field effort led by K. Taylor. The NSF Office of Polar Programs also funded the Ice Drilling Program Office and Ice Drilling Design and Operations group, the National Ice Core Laboratory, Raytheon Polar Services, and the 109th New York Air National Guard. The WD continuous CH_4 2 year fitted spline data and the experiment-time-integrated data are available at the USAP Data Centre (doi: 10.7265/N5JM27K4; http://www.usap-dc.org/view/dataset/600361). The WD2014 time scale is available here. The WD discrete CH_4 data are available here. The WD accumulation data are available (doi:10.15784/601004). The NGRIP ice core $\delta^{18}O$ 20 year mean values are available here, the Hulu cave $\delta^{18}O$ values are available here, and the Bermuda Rise SST record is here. We thank two anonymous reviewers for their constructive comments and suggestions, which have improved this manuscript.

References

Aydin, M., K. R. Verhulst, E. S. Saltzman, M. O. Battle, S. A. Montzka, D. R. Blake, Q. Tang, and M. J. Prather (2011), Recent decreases in fossil-fuel emissions of ethane and methane derived from firn air, *Nature*, *476*, 198–201, doi:10.1038/nature10352.

Bisiaux, M. M., R. Edwards, J. R. McConnell, M. A. J. Curran, T. D. Van Ommen, A. M. Smith, T. A. Neumann, D. R. Pasteris, J. E. Penner, and K. Taylor (2012), Changes in black carbon deposition to Antarctica from two high-resolution ice core records, 1850–2000 AD, *Atmos. Chem. Phys.*, *12*, 4107–4115, doi:10.5194/acp-12-4107-2012.

Brook, E. J., S. Harder, J. Severinghaus, E. J. Steig, and C. M. Sucher (2000), On the origin and timing of rapid changes in atmospheric methane during the Last Glacial Period, *Global Biogeochem. Cycles*, *14*, 559–572, doi:10.1029/1999GB001182.

Buizert, C., et al. (2015), The WAIS Divide deep ice core WD2014 chronology—Part 1: Methane synchronization (68–31 ka BP) and the gas age-ice age difference, *Clim. Past*, *11*, 153–173, doi:10.5194/cp-11-153-2015.

Chappellaz, J., et al. (2013), High-resolution glacial and deglacial record of atmospheric methane by continuous-flow and laser spectrometer analysis along the NEEM ice core, *Clim. Past*, *9*, 2579–2593, doi:10.5194/cp-9-2579-2013.

Chiang, J. C. H., and C. M. Bitz (2005), Influence of high latitude ice cover on the marine intertropical convergence zone, *Clim. Dyn.*, *25*, 477–496, doi:10.1007/s00382-005-0040-5.

Cobb, K. M., N. Westphal, H. R. Sayani, J. T. Watson, E. Di Lorenzo, H. Cheng, R. L. Edwards, and C. D. Charles (2013), Highly variable El Niño-Southern Oscillation throughout the Holocene, *Science*, *339*, 67–70, doi:10.1126/science.1228246.

Crutzen, P. J., and P. H. Zimmermann (1991), The changing photochemistry of the troposphere, *Tellus A*, *43*, 136–151, doi:10.1034/j.1600-0870.1991.00012.x.

Cuffey, K. M., G. D. Clow, E. J. Steig, C. Buizert, T. J. Fudge, M. Koutnik, E. D. Waddington, R. B. Alley, and J. P. Severinghaus (2016), Deglacial temperature history of West Antarctica, *Proc. Natl. Acad. Sci. U.S.A.*, *113*, 14,249–14,254, doi:10.1073/pnas.1609132113.

Daniau, A.-L., S. P. Harrison, and P. J. Bartlein (2010), Fire regimes during the Last Glacial, *Quat. Sci. Rev.*, *29*, 2918–2930, doi:10.1016/j.quascirev.2009.11.008.

Deplazes, G., et al. (2013), Links between tropical rainfall and North Atlantic climate during the Last Glacial Period, *Nat. Geosci.*, *6*, 213–217.

Dlugokencky, E. J., L. Bruhwiler, J. W. C. White, L. K. Emmons, P. C. Novelli, S. A. Montzka, K. A. Masarie, P. M. Lang, A. M. Crotwell, and J. B. Miller (2009), Observational constraints on recent increases in the atmospheric CH_4 burden, *Geophys. Res. Lett.*, *36*, L18803, doi:10.1029/2009GL039780.

Dlugokencky, E. J., E. G. Nisbet, R. Fisher, and D. Lowry (2011), Global atmospheric methane: Budget, changes and dangers, *Philos. Trans. A Math. Phys. Eng. Sci.*, *369*, 2058–72, doi:10.1098/rsta.2010.0341.

Etheridge, D. M., G. I. Pearman, and P. J. Fraser (1992), Changes in tropospheric methane between 1841 and 1978 from a high accumulation-rate Antarctic ice core, *Tellus B*, *44*, 282–294, doi:10.1034/j.1600-0889.1992.t01-3-00006.x.

Ferretti, D. F., et al. (2005), Unexpected changes to the global methane budget over the past 2000 years, *Science*, *309*, 1714–1717, doi:10.1126/science.1115193.

Fischer, H., S. Schüpbach, G. Gfeller, M. Bigler, R. Röthlisberger, T. Erhardt, T. F. Stocker, R. Mulvaney, and E. W. Wolff (2015), Millennial changes in North American wildfire and soil activity over the last glacial cycle, *Nat. Geosci.*, *8*, 723–727, doi:10.1038/ngeo2495.

Ford, H. L., A. C. Ravelo, and P. J. Polissar (2015), Reduced El Niño–Southern Oscillation during the Last Glacial Maximum, *Science*, *347*, 255–258, doi:10.1126/science.1258437.

García-García, D., and C. C. Ummenhofer (2015), Multidecadal variability of the continental precipitation annual amplitude driven by AMO and ENSO, *Geophys. Res. Lett.*, *42*, 526–535, doi:10.1002/2014GL062451.

Goswami, B. N., M. S. Madhusoodanan, C. P. Neema, and D. Sengupta (2006), A physical mechanism for North Atlantic SST influence on the Indian summer monsoon, *Geophys. Res. Lett.*, *33*, L02706, doi:10.1029/2005GL024803.

Gray, L. J., et al. (2010), Solar influences on climate, *Rev. Geophys.*, *48*, RG4001, doi:10.1029/2009RG000282.

Hodson, E. L., B. Poulter, N. E. Zimmermann, C. Prigent, and J. O. Kaplan (2011), The El Niño–Southern Oscillation and wetland methane interannual variability: Wetland methane emissions and ENSO, *Geophys. Res. Lett.*, *38*, L08810, doi:10.1029/2011GL046861.

Hopcroft, P. O., P. J. Valdes, and D. J. Beerling (2011), Simulating idealized Dansgaard-Oeschger events and their potential impacts on the global methane cycle, *Quat. Sci. Rev.*, *30*, 3258–3268, doi:10.1016/j.quascirev.2011.08.012.

Kaplan, J. O. (2002), Wetlands at the Last Glacial Maximum: Distribution and methane emissions, *Geophys. Res. Lett.*, *29*(6), 1079, doi:10.1029/2001GL013366.

Kerr, R. A. (2000), A North Atlantic climate pacemaker for the centuries, *Science*, *288*, 1984–1985, doi:10.1126/science.288.5473.1984.

Kindler, P., M. Guillevic, M. Baumgartner, J. Schwander, A. Landais, and M. Leuenberger (2014), Temperature reconstruction from 10 to 120 kyr b2k from the NGRIP ice core, *Clim. Past*, *10*, 887–902, doi:10.5194/cp-10-887-2014.

Kirschke, S., et al. (2013), Three decades of global methane sources and sinks, *Nat. Geosci.*, *6*, 813–823, doi:10.1038/ngeo1955.

Levine, J. G., E. W. Wolff, A. E. Jones, L. C. Sime, P. J. Valdes, A. T. Archibald, G. D. Carver, N. J. Warwick, and J. A. Pyle (2011), Reconciling the changes in atmospheric methane sources and sinks between the Last Glacial Maximum and the pre-industrial era, *Geophys. Res. Lett.*, *38*, L23804, doi:10.1029/2011GL049545.

Levine, J. G., E. W. Wolff, P. O. Hopcroft, and P. J. Valdes (2012), Controls on the tropospheric oxidizing capacity during an idealized Dansgaard-Oeschger event, and their implications for the rapid rises in atmospheric methane during the Last Glacial Period, *Geophys. Res. Lett.*, *39*, L12805, doi:10.1029/2012GL051866.

MacFarling Meure, C., D. Etheridge, C. Trudinger, P. Steele, R. Langenfelds, T. van Ommen, A. Smith, and J. Elkins (2006), Law dome CO_2, CH_4 and N_2O ice core records extended to 2000 years BP, *Geophys. Res. Lett.*, *33*, L14810, doi:10.1029/2006GL026152.

Marcott, S. A., et al. (2014), Centennial-scale changes in the global carbon cycle during the last deglaciation, *Nature*, *514*, 616–619, doi:10.1038/nature13799.

Merkel, U., M. Prange, and M. Schulz (2010), ENSO variability and teleconnections during glacial climates, *Quat. Sci. Rev.*, *29*, 86–100, doi:10.1016/j.quascirev.2009.11.006.

Mitchell, L., E. Brook, J. E. Lee, C. Buizert, and T. Sowers (2013), Constraints on the Late Holocene anthropogenic contribution to the atmospheric methane budget, *Science*, *342*, 964–966, doi:10.1126/science.1238920.

Mitchell, L. E., E. J. Brook, T. Sowers, J. R. McConnell, and K. Taylor (2011), Multidecadal variability of atmospheric methane, 1000–1800 C.E, *J. Geophys. Res.*, *116*, G02007, doi:10.1029/2010JG001441.

Möller, L., T. Sowers, M. Bock, R. Spahni, M. Behrens, J. Schmitt, H. Miller, and H. Fischer (2013), Independent variations of CH_4 emissions and isotopic composition over the past 160,000 years, *Nat. Geosci.*, *6*, 885–890, doi:10.1038/ngeo1922.

Montzka, S. A., M. Krol, E. J. Dlugokencky, B. Hall, P. Jöckel, and J. Lelieveld (2011), Small interannual variability of global atmospheric hydroxyl, *Science*, *331*, 67–69, doi:10.1126/science.1197640.

Murray, L. T., L. J. Mickley, J. O. Kaplan, E. D. Sofen, M. Pfeiffer, and B. Alexander (2014), Factors controlling variability in the oxidative capacity of the troposphere since the Last Glacial Maximum, *Atmos. Chem. Phys.*, *14*, 3589–3622.

Myhre, G., et al. (2013), Anthropogenic and natural radiative forcing contribution of working group I to the fifth assessment report of the Intergovernmental Panel on Climate Change, in *Climate Change 2013: The Physical Science Basis. Contribution of Working Group I to the Fifth Assessment Report of the Intergovernmental Panel on Climate Change*, edited by T. F. Stocker et al., Cambridge Univ. Press, Cambridge, U. K., and New York.

Neff, U., S. J. Burns, A. Mangini, M. Mudelsee, D. Fleitmann, and A. Matter (2001), Strong coherence between solar variability and the monsoon in Oman between 9 and 6 kyr ago, *Nature*, *411*, 290–293.

Nisbet, E. G., E. J. Dlugokencky, and P. Bousquet (2014), Methane on the rise—Again, *Science*, *343*, 493–495, doi:10.1126/science.1247828.

Nisbet, E. G., et al. (2016), Rising atmospheric methane: 2007–2014 growth and isotopic shift, *Global Biogeochem. Cycles*, *30*, 1356–1370, doi:10.1002/2016GB005406.

Rasmussen, S. O., et al. (2013), A first chronology for the North Greenland Eemian ice drilling (NEEM) ice core, *Clim. Past*, *9*, 2713–2730, doi:10.5194/cp-9-2713-2013.

Rhodes, R. H., X. Faïn, C. Stowasser, T. Blunier, J. Chappellaz, J. R. McConnell, D. Romanini, L. E. Mitchell, and E. J. Brook (2013), Continuous methane measurements from a late Holocene Greenland ice core: Atmospheric and in-situ signals, *Earth Planet. Sci. Lett.*, *368*, 9–19, doi:10.1016/j.epsl.2013.02.034.

Rhodes, R. H., E. J. Brook, J. C. Chiang, T. Blunier, O. J. Maselli, J. R. McConnell, D. Romanini, and J. P. Severinghaus (2015), Enhanced tropical methane production in response to iceberg discharge in the North Atlantic, *Science*, *348*, 1016–1019.

Rhodes, R. H., et al. (2016), Local artifacts in ice core methane records caused by layered bubble trapping and in situ production: A multi-site investigation, *Clim. Past*, *12*, 1061–1077, doi:10.5194/cp-12-1061-2016.

Rice, A. L., C. L. Butenhoff, D. G. Teama, F. H. Röger, M. A. K. Khalil, and R. A. Rasmussen (2016), Atmospheric methane isotopic record favors fossil sources flat in 1980s and 1990s with recent increase, *Proc. Natl. Acad. Sci. U.S.A.*, *113*, 10,791–10,796, doi:10.1073/pnas.1522923113.

Rosen, J. L., E. J. Brook, J. P. Severinghaus, T. Blunier, L. E. Mitchell, J. E. Lee, J. S. Edwards, and V. Gkinis (2014), An ice core record of near-synchronous global climate changes at the Bølling transition, *Nat. Geosci.*, *7*, 459–463, doi:10.1038/ngeo2147.

Sachs, J. P., and S. J. Lehman (1999), Subtropical North Atlantic temperatures 60,000 to 30,000 years ago, *Science*, *286*, 756–759, doi:10.1126/science.286.5440.756.

Sapart, C. J., et al. (2012), Natural and anthropogenic variations in methane sources during the past two millennia, *Nature*, *490*, 85–8, doi:10.1038/nature11461.

Saunois, M., et al. (2016), The global methane budget 2000–2012, *Earth Syst. Sci. Data*, *8*, 697–751, doi:10.5194/essd-8-697-2016.

Schaefer, H., et al. (2016), A 21st century shift from fossil-fuel to biogenic methane emissions indicated by $^{13}CH_4$, *Science*, *352*(6281), 80–4, doi:10.1126/science.aad2705.

Schulz, M., and M. Mudelsee (2002), REDFIT: Estimating red-noise spectra directly from unevenly spaced paleoclimate time series, *Comput. Geosci.*, *28*, 421–426.

Schwander, J., T. Sowers, J. M. Barnola, T. Blunier, A. Fuchs, and B. Malaizé (1997), Age scale of the air in the summit ice: Implication for glacial-interglacial temperature change, *J. Geophys. Res.*, *102*, 19,483–19,493, doi:10.1029/97JD01309.

Schwietzke, S., et al. (2016), Upward revision of global fossil fuel methane emissions based on isotope database, *Nature*, *538*, 88–91, doi:10.1038/nature19797.

Seierstad, I. K., et al. (2014), Consistently dated records from the Greenland GRIP, GISP2 and NGRIP ice cores for the past 104 ka reveal regional millennial-scale $\delta^{18}O$ gradients with possible Heinrich event imprint, *Quat. Sci. Rev.*, *106*, 29–46, doi:10.1016/j.quascirev.2014.10.032.

Sigl, M., et al. (2016), The WAIS Divide deep ice core WD2014 chronology—Part 2: Annual-layer counting (0–31 kaBP), *Clim. Past*, *12*, 769–786, doi:10.5194/cp-12-769-2016.

Sperlich, P., H. Schaefer, S. E. Mikaloff Fletcher, M. Guillevic, K. Lassey, C. J. Sapart, T. Röckmann, and T. Blunier (2015), Carbon isotope ratios suggest no additional methane from boreal wetlands during the rapid Greenland Interstadial 21.2, *Global Biogeochem. Cycles*, *29*, 1962–1976, doi:10.1002/2014GB005007.

Stowasser, C., et al. (2012), Continuous measurements of methane mixing ratios from ice cores, *Atmos. Meas. Tech.*, *5*, 999–1013, doi:10.5194/amt-5-999-2012.

Tierney, J. E., N. J. Abram, K. J. Anchukaitis, M. N. Evans, C. Giry, K. H. Kilbourne, C. P. Saenger, H. C. Wu, and J. Zinke (2015), Tropical sea surface temperatures for the past four centuries reconstructed from coral archives, *Paleoceanography*, *30*, 226–252, doi:10.1002/2014PA002717.

van der Werf, G. R., J. T. Randerson, L. Giglio, G. J. Collatz, P. S. Kasibhatla, and A. F. Arellano Jr. (2006), Interannual variability in global biomass burning emissions from 1997 to 2004, *Atmos. Meas. Tech.*, *6*, 3423–3441.

West Antarctic Ice Sheet (WAIS) Divide Project Members (2015), Precise interpolar phasing of abrupt climate change during the last ice age, *Nature*, *520*, 661–665, doi:10.1038/nature14401.

Zhang, R., and T. L. Delworth (2006), Impact of Atlantic multidecadal oscillations on India/Sahel rainfall and Atlantic hurricanes, *Geophys. Res. Lett.*, *33*, L17712, doi:10.1029/2006GL026267.